Ab initio lattice dynamics of BN and AlN: Covalent versus ionic forces

Krystian Karch and Friedhelm Bechstedt
Friedrich-Schiller-Universität, Institut für Festkörpertheorie und Theoretische Optik, Max-Wien-Platz 1, D-07743 Jena, Germany
(Received 6 January 1997; revised manuscript received 13 June 1997)

We report first-principles calculations of the structural, lattice-dynamical, and dielectric properties for zinc-blende and wurtzite BN and AlN. The ground-state properties, i.e., the lattice constants, the bulk moduli, the ionicity factors of the chemical bonds, and the elastic constants, are calculated using a plane-wave-pseudopotential method within the density-functional theory. A linear-response approach to the density-functional theory is used to derive the Born effective charges, the high-frequency dielectric constants, and the phonon frequencies and eigenvectors. The different behavior of the structural and lattice-dynamical properties of BN and AlN is discussed in terms of the different ionicities, strengths of the covalent bonds, and the atomic masses. Our results are in excellent agreement with the experimental data available. [S0163-1829(97)06736-2]

I. INTRODUCTION

Among the III-V semiconductors the nitrides (BN, AlN, and GaN) have attracted both scientific and technological interest in recent years. This is due to the fascinating mechanical properties of their zinc-blende and/or wurtzite phases, such as hardness, high melting point, high thermal conductivity, large bulk moduli, etc., making them useful for protective coatings. Furthermore, the electronic properties, characterized by large band gaps and relatively low dielectric constants, indicate potential device applications in ultraviolet optics and high-temperature microelectronics. These outstanding properties are mainly related to the specific role of the nitrogen atoms. The smallness of the nitrogen atoms gives rise to the formation of short bonds, which leads to significantly smaller lattice constants (by 20–40%) than in other III-V semiconductors like GaAs or InAs.

Boron and nitrogen lie on both sides of carbon in the periodic table and their average mass is almost the same as the mass of carbon. Therefore, the physical, mechanical, and chemical properties of BN compounds are expected to be close to those of the carbon polymorphs. At ambient conditions, BN crystallizes usually in a hexagonal structure with a two-layer stacking sequence that is analogous to that of graphite, but a rhombohedral form with a three-layer stacking also exists.[1] The denser zinc-blende and wurtzite phases of BN that are similar to cubic and hexagonal diamond are thermodynamically stable at high pressure and high temperature.[2] The number of bilayers of cations and anions, defining the translational symmetry parallel to the cubic [111] or hexagonal [0001] direction, varies from 3 to 2. Consequently, the cubic (hexagonal) zinc-blende (wurtzite) structure is denoted by $3C$ $(2H)$.

The more ionic compound AlN, which is generally reported to be nonpolymorphous, crystallizes at ambient condition in the wurtzite structure.[3] However, several works report the occurrence of a metastable zinc-blende polytype of AlN.[4] Because of the reactivity of AlN, high-purity source material and an oxygen-free environment are required to grow AlN crystals of good quality. Therefore, AlN is not a particular easy material to study experimentally and most researchers in the field have concentrated on GaN. The position of the aluminum and the nitrogen atom in the periodic table indicates that the physical properties of AlN should be similar to those of SiC.

In this paper we present an extensive *ab initio* study of the ground-state (lattice constants, internal cell parameters, bulk moduli), lattice-dynamical (phonon frequencies and eigenvectors), and dielectric properties (Born effective charges and dielectric constants) of BN and AlN semiconductors in both wurtzite and zinc-blende structures. We focus our attention on the differences in the bonding properties between these phases as well as on the contributions of the cations boron and aluminum to the ionic/covalent character of the bonds in the considered compounds. The paper is organized as follows. In Sec. II we briefly review the theoretical method used. In Sec. III the results of our calculations are presented and discussed. Finally, conclusions are given in Sec. IV.

II. COMPUTATIONAL DETAILS

Our calculations are performed using the plane-wave pseudopotential approach within the framework of the density-functional theory (DFT). Electronic exchange and correlation energies are calculated within the the local-density approximation (LDA) using a standard form for the exchange-correlation potential.[5] Electron-ion interactions are evaluated using nonlocal, norm-conserving pseudopotentials generated using the scheme proposed by Troullier and Martins.[6] We paid particular attention to the choice of the reference configuration for the excited atomic d states. The Troullier and Martins procedure yields soft-core pseudopotentials that greatly reduce the number of plane waves needed to achieve convergence in the calculated properties.[7] The summation over the Brillouin zone (BZ) is done using sets of Chadi-Cohen special points.[8] Since the crystal structures considered here are semiconducting convergence is reached using 12 (10) special points in the irreducible wedge of BZ of the wurtzite (zinc-blende) structure.

The ground-state properties of the zinc-blende (wurtzite) structure are obtained by minimization of the total energy with respect to the unit-cell volume V (lattice constants a and c and the internal parameters u). For the wurtzite struc-

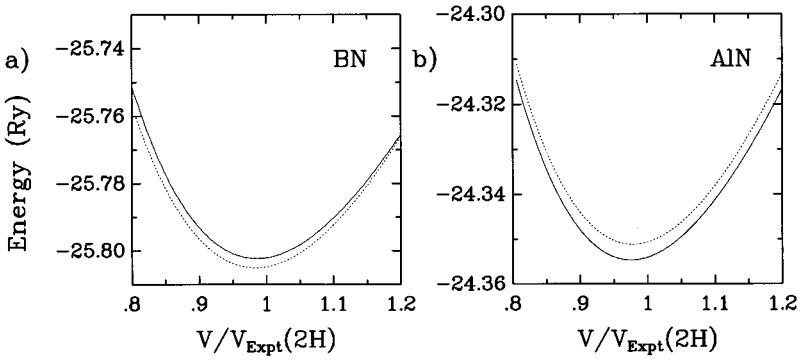

FIG. 1. Calculated total energies per molecule for BN (a) and AlN (b) versus reduced volume. The solid (dotted) line indicates the total energy of the wurtzite (zinc-blende) structure.

ture this minimization has been performed by a two-step procedure. For a given unit-cell volume $V=\sqrt{3}a^2c/2$, the total energy was minimized with respect to c/a and u. This step was repeated for other volumes near the experimental equilibrium one. The theoretical equilibrium volume V_0, the static bulk modulus at zero pressure B_0, and the first-order pressure derivative of the bulk modulus B_0' have been finally determined by fitting the calculated static total energies as a function of volume to the Vinet equation of state.[9] The lattice-dynamical properties, i.e., phonon frequencies and eigenvectors, are calculated within the framework of the self-consistent density-functional perturbation theory (DFPT).[10–13] DFPT also allows the calculation of the high-frequency dielectric tensor ϵ_∞ and of the Born effective charge tensor $\mathbf{Z}^{\mathrm{B}}$ for each inequivalent atom in the unit cell. These quantities are necessary for the nonanalytic part of the dynamical matrix of the polar semiconductors BN and AlN.

The single-particle electronic eigenfunctions solving the Kohn-Sham equations of the DFT-LDA are expanded in terms of plane waves. Because the nitrogen core does not possess p states, p-like valence electrons are strongly localized in the core region. Hence, the p component of the nonlocal nitrogen pseudopotential is relatively deep in the core region and the plane-wave expansion requires a high kinetic-energy cutoff for good convergence. In the present work, plane waves up to 50 Ry are used for the calculation of the structural and dynamical properties of AlN ensuring the convergence of the calculated phonon frequencies to within 3 cm^{-1}. Because of the lack of p-core states in boron and the smaller unit-cell volume of BN than of AlN the same quality of convergence for the dynamical properties of BN is reached using the cutoff energy of 60 Ry.

III. RESULTS AND DISCUSSION

A. Ground-state properties

The calculated ground-state energies plotted as functions of volume for $3C$ and $2H$ BN and AlN are shown in Fig. 1. In Table I, the calculated structural, elastic, and cohesive properties as obtained from the Vinet EOS are compared with experimental values. The calculated structural properties of both semiconductors are in good agreement with the

TABLE I. Comparison of calculated and measured structural properties of BN and AlN in zinc-blende and wurtzite phases: lattice constant a (Å), ratio c/a, internal parameter u, bulk modulus B_0 (Mbar) and its pressure derivative B_0', ionicity coefficient g, and total energy difference $\Delta\mathcal{E}$ (meV/molecule) with respect to the zinc-blende structure.

		a	c/a	u	B_0	B_0'	g	$\Delta\mathcal{E}$
$3C$ BN	Calc.	3.591			3.97	3.6	0.491	
	Calc. [a]	3.576			3.97	3.6		
	Calc. [b]	3.575			3.86			
	Expt. [c]	3.615			3.69	4.0		
$2H$ BN	Calc.	2.531	1.657	0.3751	3.99	3.6	0.492	37
	Calc. [a]	2.521	1.632		4.01	3.6		20
	Expt.	2.553[d]	1.656[d]		4.10[e]			
$3C$ AlN	Calc.	4.337			2.14	3.3	0.796	
	Calc. [f]	4.316			2.15	4.6		
	Expt. [g]	4.380						
$2H$ AlN	Calc.	3.082	1.605	0.3816	2.15	3.6	0.794	−48
	Calc. [f]	3.129	1.594	0.3825	1.95	3.7		
	Expt.	3.110[h]	1.601[h]	0.3821[h]	2.08[i]	6.3[i]		

[a]Reference 17.
[b]Reference 18.
[c]Reference 15.
[d]Reference 14.
[e]Reference 17.
[f]Reference 30.
[g]Reference 18.
[h]Reference 16.
[i]Reference 19.

room-temperature experimental data of Soma *et al.*[14] and Knittle *et al.*[15] for BN and Schulz *et al.*[16] for AlN. The static bulk moduli of both materials are overestimated by the theory, in case of BN by about 8% while for AlN the experimental value is exceeded by about 3%. The present determined value of the bulk modulus of BN is, however, in good agreement with the recent results of Furthmüller *et al.*[20] and of Rodriguez-Hernandez *et al.*[21] Moreover, it has been recently shown[22,23] that anharmonic corrections due to phonon vibrational energy may considerably reduce the value of the static bulk modulus, even at $T=0$ K. The zero-point motional energy lowers the value of the static bulk modulus of diamond[22] (cubic silicon carbide[23]) by 3% (2%). One should also notice that the experimental values of the bulk moduli are somehow uncertain due to the difficulty of growing high-quality single crystals of III-V nitrides.

Despite the formal similarities of both materials, the stable phase varies from zinc-blende (BN) to wurtzite (AlN). The energy loss (gain) calculated for the wurtzite BN (AlN) with respect to the zinc-blende structure is with $\Delta\mathcal{E}=37$ meV (-48 meV), very close to the values calculated recently by other authors using plane-wave pseudopotential methods.[20,24,25] Previous calculations[26–31] gave the same trend, however, with a wide spread of values for $\Delta\mathcal{E}$. For a given A^NB^{8-N} compound the stability of the wurtzite structure relative to the zinc-blende structure can also be discussed in terms of the critical parameter $\Delta(c/a)$, defined as the deviation $\Delta(c/a)=c/a-\sqrt{8/3}$ of the ratio c/a from its ideal value.[32] The zinc-blende (wurtzite) structure prevails when $\Delta(c/a)$ is positive (negative). Therefore, the value of the calculated critical parameter $\Delta(c/a)=+0.024$ for $2H$ BN (-0.029 for $2H$ AlN) correlates well with the calculated energy gain $\Delta\mathcal{E}$. Moreover, the critical parameter $\Delta(c/a)$ can be related to the ionicity of a compound. In general, A^NB^{8-N} wurtzite compounds with relatively large negative values of $\Delta(c/a)$ exhibit strong ionic bonding properties.[32] Thus AlN is a more ionic compound than BN (see Table I). Furthermore, the deviations from the ideal wurtzite structure of $2H$ AlN suggest that this stable compound may exhibit a large permanent macroscopic polarization, i.e., pyroelectricity. Such a polarization may influence the interface properties of $2H$ AlN with its cubic $3C$ phase or with other semiconductors as has been shown for the heterocrystalline combination of $2H$ and $3C$ SiC (Ref. 33) or for the band discontinuities of AlN with GaN.[25]

Unlike the zinc-blende case, in the wurtzite structure there are two different nearest-neighbor bonds: one along the c direction with the bond length $R^{(1)}=uc$ and three equal bonds forming hexagonal layers with the bond length $R^{(2)}=a\sqrt{1/3+(1/2-u)^2(c/a)^2}$. For most stable wurtzite-type structures c/a ratio and the u parameter are strongly correlated; If c/a decreases, then u increases in such a way that the inequivalent bond lengths $R^{(1)}$ and $R^{(2)}$ are nearly equal, however, the tetrahedral angles are distorted. The bond lengths $R^{(1)}$ and $R^{(2)}$ would be equal if $u=a^2/(3c^2)+1/4$. The so-estimated value of the internal parameter u of $2H$ AlN (0.3794) nearly agrees with the calculated one (0.3816). In the case of $2H$ BN there is, however, a larger deviation between the estimated value (0.3714) and the calculated one (0.3751), which is in fact almost the ideal value (0.375). This finding can be attributed to the strong covalent sp^3 bonding of $2H$ BN, which preserves the ideal tetrahedral bond angles.

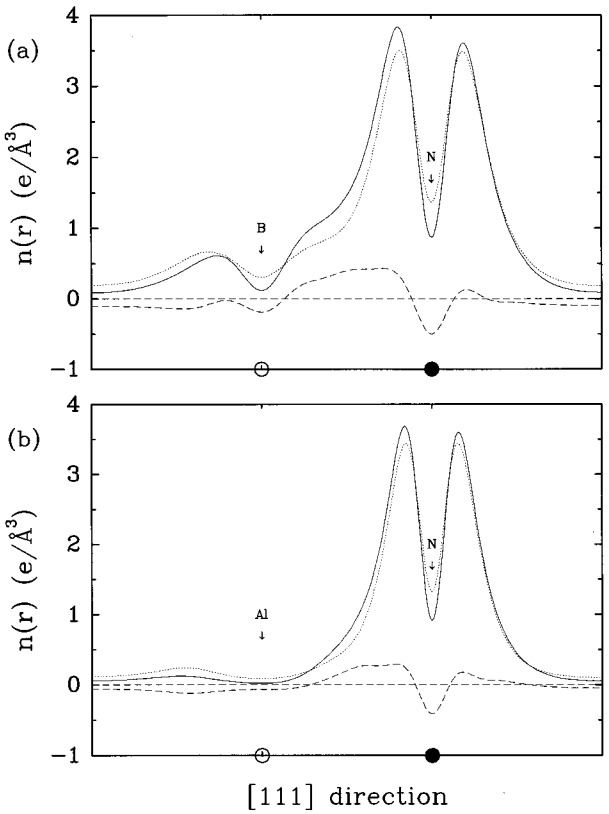

FIG. 2. Line plots of the valence-charge density of $3C$ BN (a) and AlN (b) along the [111] direction. The self-consistent electron charge density is indicated by solid lines, the superposition of the atomic valence charges by dotted lines, and the difference between both by dashed lines.

The electronic charge density of BN and AlN differs considerably from that of other III-V semiconductors like GaAs or InP. This is apparent from the line plots of the valence-charge density of both compounds along the [111] direction shown in Fig. 2. The overall shape of the valence-charge density suggests a highly ionic B^+N^- or Al^+N^- bonding. In order to characterize the degree of the ionic versus the covalent contribution to the bond the charge redistribution $\Delta\rho$ has been calculated with respect to the superposition of free-atom charge densities. The positive (negative) charge redistribution can be identified with electron transfer into *bonding* (*antibonding*) electronic states. Moreover, the ionic component of the bonding can be identified with the charge transfer from the cation to the anion, while the deviation of the charge density from spherical symmetry indicates the covalent nature of the bonding. Although there is no visible *bond charge* in the electronic charge density of BN and AlN as in the case of typical covalent III-V semiconductors, the remarkable increase of the charge density along the bond direction indicates a strong covalent bonding that stabilizes both crystals.

Recently, Garcia and Cohen introduced a first-principles ionicity scale for binary cubic A^NB^{8-N} compounds.[34] As this ionicity approach is based on the ground-state valence-charge density, it describes the *static* ionicity of a compound.

Within this approach the ionicity parameter g is defined in terms of the symmetric/antisymmetric ($\rho_{S/A}$) parts of the charge density with respect to the bond center as $g=\sqrt{S_A/S_S}$, where the integrated quantity $S_{S/A}=1/V_0\int\rho_{S/A}^2(\mathbf{r})d\mathbf{r}$ measures the strength of $\rho_{S/A}$. For cubic structures this parameter g is uniquely defined. In the wurtzite structure, however, there are two different bonds $R^{(1)}$ and $R^{(2)}$. For this structure the decomposition of the valence-charge density into symmetric and antisymmetric parts is proper only for the $R^{(2)}$ bond center at which inversion maps cations into anions and vice versa.[35] The different ionicities of the chemical bonds in AlN and BN can be already seen from the representation of the valence-charge density along the bond direction as shown in Fig. 2. In comparison to the B atom in BN the probability to find valence electrons around the Al atom in AlN is much lower. The obtained static ionicity values of 3C BN ($g=0.491$) and 3C AlN ($g=0.796$) confirm this qualitative finding. The values of the ionicity parameter g for the wurtzite structures of both semiconductors are almost identical to those of the zinc-blende structures (see Table I). As can be seen in Fig. 2, the significant part of the asymmetric valence-charge density is already given by the superposition of the atomic charges. The ionicity of both compounds is, therefore, based on the intrinsic differences between the valence-charge densities of the constituent ions.

B. Elastic properties

The linear elastic constants $\boldsymbol{c}$ are formally defined as $c_{\alpha\beta,\gamma\delta}=\partial\sigma_{\alpha\beta}/\partial\eta_{\gamma\delta}$, where $\boldsymbol{\eta}$ denotes the applied strain. The fourth-rank tensor $\boldsymbol{c}$ possesses generally 21 independent components. However, this number is greatly reduced when taking into account the symmetry of the crystal. In the case of cubic crystals symmetry relations reduce the number of independent components to three: $c_{11}=c_{xx,xx}$, $c_{12}=c_{xx,yy}$, and $c_{44}=c_{yz,yz}$. The elastic constants c_{11} and c_{12} and the unrelaxed constant $c_{44}^{(0)}$ have been calculated by computing the components of the stress tensor $\boldsymbol{\sigma}$ for small applied tetragonal and trigonal strains $\boldsymbol{\eta}$ (less then 3%), using the approach proposed by Nielson and Martin.[36] The calculation of the elastic constants directly from the total energy requires more extensive calculations because the total energy differences between the strained and the unstrained configurations are only of the order of a few mRy.[37] The unrelaxed $c_{44}^{(0)}$ and the relaxed elastic constant c_{44} are related by

$$c_{44}=c_{44}^{(0)}-\frac{1}{4a}\mu\omega_{\mathrm{TO}}^2(\Gamma)\zeta^2, \tag{1}$$

where μ is the reduced atomic mass, $\omega_{\mathrm{TO}}(\Gamma)$ denotes the transverse zone-center phonon frequency, and ζ is the internal-strain parameter. The internal-strain parameter ζ that describes the sublattice displacement due to the applied macroscopic strain $\boldsymbol{\eta}$ is the only one independent component of the third-rank internal-strain tensor $\boldsymbol{\Delta}$ for diamond and zinc-blende structures.[38] The internal-strain parameter can be computed from the derivative of the strain $\boldsymbol{\sigma}$ with respect to the displacement $\boldsymbol{u}$ of one atom in the unit cell,[12]

TABLE II. Values of the relaxed c_{ij} and unrelaxed elastic constants $c_{44}^{(0)}$ (Mbar) and of the internal-strain parameter ζ for 3C BN and AlN.

		c_{11}	c_{12}	c_{44}	$c_{44}^{(0)}$	ζ
3C BN	Present	8.12	1.82	4.64	4.66	0.07
	Expt. [a]	8.20	1.90	4.80		
	Calc. [b]	7.12	0.80	2.90		
	Calc. [c]	8.31	4.20	4.50		
	Calc. [d]	8.44	1.90	4.83	4.86	0.11
	Calc. [e]	8.37	1.82	4.93	4.95	0.10
3C AlN	Present	2.94	1.60	1.89	2.33	0.57
	Calc. [f]	3.48	1.68	1.35		
	Calc. [e]	3.04	1.52	1.99	2.30	0.60

[a]Brillouin scattering, Grimsditch *et al.* (Ref. 40).
[b]Semiempirical, De Vries (Ref. 42).
[c]Semiempirical, Sokolovskii (Ref. 41).
[d]Pseudopotential, Rodriguez-Hernandez *et al.* (Ref. 21).
[e]LMTO, Kim *et al.* (Ref. 43).
[f]Hartree-Fock, Ruiz *et al.* (Ref. 44).

$$\zeta=\frac{a}{\mu\omega_{\mathrm{TO}}^2(\Gamma)}\left(\frac{\partial\sigma_{yz}}{\partial u_x}\right)_{\boldsymbol{\eta}=0}. \tag{2}$$

For this calculation the anion at the origin of the unit cell has been kept fixed, while the cation at the tetrahedral position of one quarter of the body diagonal has been displaced along the [111] direction. Such a displacement reduces the number of symmetry operations from 24 to 6 but preserves the cubic symmetry of the lattice. A more detailed description of the method used can be found in Refs. 12 and 39.

The theoretical values of the elastic constants and of the internal-strain parameters of 3C BN and AlN are summarized in Table II. Experimental data for the elastic constants are only available for 3C BN. Excellent agreement is observed for the elastic constants of BN with recent experimental data obtained from Brillouin scattering measurements.[40] Former data derived using semiempirical methods are found to be rather inaccurate.[41,42] Our elastic constants of 3C BN are also in good agreement with recent pseudopotential[21] and full-potential linear-muffin-tin-orbital (LMTO) calculations.[43] This holds also for the elastic constants of 3C AlN in comparison with the Hartree-Fock[44] and LMTO (Ref. 43) values. If we assume that the ions forming the crystal lattice are bound only by central forces, then additional relations, the so-called Cauchy relations, exist between the elastic constants. For cubic crystals there is only one relation: $c_{12}=c_{44}$. It is evident from Table II that this equality holds neither for 3C BN nor for 3C AlN. However, this relation is more strongly violated for BN ($c_{12}/c_{44}=1.75$) than for AlN ($c_{12}/c_{44}=1.51$). The violation of the Cauchy condition indicates the presence of considerable noncentral forces arising from the covalent bonding. This noncentral forces turns out to be stronger in BN than in AlN.

To the best of our knowledge, no experimental data for the internal-strain parameter of both semiconductors AlN and BN are available. Although our calculated internal-strain parameters of 3C BN and AlN are in good agreement with recent pseudopotential[21] and LMTO (Ref. 43) calculations,

their absolute values are slightly smaller than the previously calculated ones. The internal-strain parameter of BN, $\zeta=0.073$, is much smaller than that of AlN, $\zeta=0.568$, indicating again a quite different bonding in the considered semiconductors. The small value of ζ for BN points out that in this material there is a large resistance against bond-bending distortions. Such an importance of bond-bending forces is characteristic for systems with strong covalent bonding and strongly localized charge-density-like diamond.[12] The experimental (theoretical) value of ζ found for diamond is 0.125 (Ref. 45) [0.116 (Ref. 39)]. In systems with weaker bound electrons and with partially ionic/covalent bonding, where lattice distortions are accompanied with relatively large charge density redistributions, larger values are observed for ζ, e.g., $\zeta=0.76$ for GaAs.[46] In order to corroborate the obtained values of ζ by an independent method we compute ζ from the derivative of the internal forces acting on the atoms in the unit cell with respect to the applied uniform stress along the [111] direction.[47] Following this procedure, we derived $\zeta=0.068$ for $3C$ BN and $\zeta=0.567$ for $3C$ AlN. Both results agree well with the values obtained from strain-displacement relation [see Eq. (2)] and, therefore, confirm the consistency of our calculations.

The elastic constants of the ideal wurtzite and zinc-blende structures may be considered as correlated because the two structures are identical up to the second-nearest neighbors. Both crystal structures can be constructed from identical tetrahedral building blocks. A procedure for relating the elastic constants of the zinc-blende to the wurtzite crystal based on this structural similarity has been developed by Martin.[48] Martin's procedure consists of applying a rotation of the elastic tensor of the zinc-blende to the elastic tensor of the hexagonal structure. In addition, a correction term to this rotation due to the internal-strain effects has to be taken into account.[48] The details of this method have been recently discussed by Kim *et al.*[43] A second independent set of equations for the transformation of the elastic constants from zinc-blende to hexagonal structure is given in Ref. 49. Our results for the elastic constants C_{ij} of the wurtzite structure of BN and AlN obtained using the above-mentioned procedures are given in Table III. The agreement with the experimental data[50,51] and with other first-principles calculations[43,44] is reasonable. However, it should be noticed that both transformation procedures assume ideal wurtzite structure neglecting the relaxation of the lattice constants ratio c/a and the internal parameter u from their ideal values. Therefore, the most discrepancies between the theoretical and the experimental values of the elastic constants may be traced back to the neglect of these structural relaxations.

TABLE III. Calculated and experimental elastic constants C_{ij} (Mbar) of wurtzite BN and AlN.

		C_{11}	C_{12}	C_{13}	C_{33}	C_{44}	C_{66}
$2H$ BN	Present [a]	9.44	1.49	0.83	10.11	3.50	3.98
	Present [b]	9.47	1.46	0.83	10.11	3.47	4.01
	Calc. [c]	9.87	1.43	0.70	10.20	3.69	4.22
$2H$ AlN	Present [a]	4.10	1.25	0.79	4.57	1.04	1.43
	Present [b]	3.85	1.50	0.79	4.57	1.08	1.18
	Expt. [d]	3.45	1.25	1.20	3.95	1.18	1.10
	Expt. [e]	4.11	1.49	0.99	3.89	1.25	1.31
	Calc. [c]	3.98	1.40	1.27	3.82	0.96	1.29
	Calc. [f]	4.64	1.49	1.16	4.09	1.28	1.48

[a]Calculated from cubic elastic constants using transformation set from Ref. 48.
[b]Calculated from cubic elastic constants using transformation set from Ref. 49.
[c]LMTO, Kim *et al.* (Ref. 43).
[d]Surface acoustic wave velocity, Tsubouchi *et al.* (Ref. 51).
[e]Brillouin scattering, McNeil *et al.* (Ref. 50).
[f]Hartree-Fock, Ruiz *et al.* (Ref. 44).

C. Dielectric properties

The interest in the macroscopic dielectric tensor $\epsilon(\infty)$ and the Born effective charge tensors $\mathbf{Z}^{\mathrm{B}}(\kappa)$ is motivated by the study of the lattice dynamics of the polar semiconductors BN and AlN. Contrary to the nonpolar IV-IV element crystals, atomic displacements in polar materials create dipoles, which give rise to long-range force constants in real space and to the nonanalytic behavior of the dynamical matrix in the limit $\mathbf{q}\rightarrow 0$. The macroscopic dielectric tensor $\epsilon(\infty)$ is formally defined as

$$\epsilon_{\alpha\beta}(\infty)=1+4\pi\frac{\partial P_\alpha}{\partial E_\beta}, \tag{3}$$

where $\mathbf{P}$ is the macroscopic electronic polarization induced by the screened electric field $\mathbf{E}$. On the other hand, the tensor of the Born effective charges

$$Z^{\mathrm{B}}_{\alpha\beta}(\kappa)=\frac{V}{e}\frac{\partial P_\alpha}{\partial u_\beta(\kappa)} \tag{4}$$

is a measure of the polarization induced by a displacement $\mathbf{u}$ of the κth atom at vanishing electric field.

In Table IV we compare the calculated dielectric tensor $\epsilon(\infty)$ of BN and AlN in the zinc-blende and wurtzite structure with experimental values available. In case of cubic symmetry $\epsilon(\infty)$ has a diagonal form and possesses only one independent component $\epsilon(\infty)=\epsilon_{xx}(\infty)=\epsilon_{yy}(\infty)=\epsilon_{zz}(\infty)$. For the wurtzite structure $\epsilon(\infty)$ is composed of two independent components, one corresponding to the direction parallel to the c axis, $\epsilon_{||}(\infty)=\epsilon_{zz}(\infty)$, and the other being characteristic for the hexagonal plane perpendicular to the c axis, $\epsilon_{\perp}(\infty)=\epsilon_{xx}(\infty)=\epsilon_{yy}(\infty)$. The average dielectric tensor $\epsilon(\infty)=1/3\ \mathrm{Tr}\epsilon(\infty)$ is also included in Table IV. Our theoretical results for $\epsilon(\infty)$ are in good agreement with experiments.[52–54] However, one should note that the experimental data available for the stable structures of BN and AlN are scarce and may suffer from the relatively low quality of the crystal samples. This concerns especially AlN where our calculations underestimate the measured average dielectric tensor of $2H$ AlN.[53,54] Previous computations on IV-IV element crystals[10] as well as on III-V (Ref. 12) and II-VI (Ref. 55) semiconductors show that the screening tends to be overestimated in theoretical calculations performed within the LDA approximation. Therefore, we guess that this unusual LDA underestimation of the dielectric tensor of $2H$ AlN with respect to the measured data may be traced back to the poor quality of $2H$ AlN samples used in the IR reflectivity measurements.[53,54]

TABLE IV. Macroscopic dielectric tensor $\epsilon(\infty)$ and Born effective charge Z^B of BN and AlN in zinc-blende and wurtzite structures. The present calculation of $\epsilon(\infty)$ includes local-field corrections.

		$\epsilon_\perp(\infty)$	$\epsilon_{\|\|}(\infty)$	$\epsilon(\infty)$	$\Delta\epsilon(\infty)$	$Z^B_\perp$	$Z^B_{\|\|}$	Z^B	ΔZ^B
3*C* BN	Present	4.54	4.54	4.54		1.93	1.93	1.93	
	Expt.			4.46[a]				1.98[b]	
	Calc. [c]	3.86	3.86	3.86					
	Calc. [d]	4.14	4.14	4.14					
	Calc. [e]	4.56	4.56	4.56					
2*H* BN	Present	4.50	4.67	4.56	0.037	1.86	1.96	1.89	0.053
	Calc. [c]	4.16	4.18	4.17	0.004				
	Calc. [d]	4.19	4.06	4.14	−0.031				
	Calc. [e]	4.51	4.69	4.57	0.039				
	Calc. [f]	3.98	4.23	4.07	0.061				
3*C* AlN	Present	4.46	4.46	4.46		2.56	2.56	2.56	
	Calc. [d]	3.90	3.90	3.90					
	Calc. [e]	4.61	4.61	4.61					
2*H* AlN	Present	4.38	4.61	4.46	0.052	2.53	2.69	2.58	0.062
	Expt.			4.84[g]				2.57[b]	
	Expt. [h]			4.68					
	Calc. [d]	3.91	3.77	3.86	−0.036				
	Calc. [e]	4.42	4.70	4.51	0.062				
	Calc. [f]	3.88	5.06	4.27	0.276				

[a]IR spectra, Eremets *et al.* (Ref. 52).
[b]First-order Raman spectra, Sanjurjo *et al.* (Ref. 63).
[c]OLCAO (without local-field corrections), Xu *et al.* (Ref. 29).
[d]LMTO (without local-field corrections), Christensen *et al.* (Ref. 57).
[e]Pseudopotential (with local-field corrections), Chen *et al.* (Ref. 58).
[f]OLCAO (without local-field corrections), Xu *et al.* (Ref. 56).
[g]IR reflectivity, Collins *et al.* (Ref. 53).
[h]IR reflectivity, Akasaki *et al.* (Ref. 54).

The degree of the anisotropy of $\epsilon(\infty)$ for the wurtzite structure can be estimated from the difference between $\epsilon_{||}(\infty)$ and $\epsilon_\perp(\infty)$: $\Delta\epsilon(\infty)=[\epsilon_{||}(\infty)-\epsilon_\perp(\infty)]/\epsilon(\infty)$. For the analysis of the reflectivity data of 2*H* AlN, Collins *et al.*[53] and Akasaki *et al.*[54] assumed an isotropy of the dielectric tensor. Hence, the degree of the uniaxial anisotropy for $\epsilon(\infty)$ of 2*H* AlN implied by the wurtzite structure has not been experimentally resolved. To the best of our knowledge, no experimental data exist for $\epsilon(\infty)$ of 2*H* BN. The calculated ratio $\Delta^{\mathrm{AlN}}\epsilon(\infty)/\Delta^{\mathrm{BN}}\epsilon(\infty)=1.405$ indicates that the wurtzite structure of AlN exhibits higher dielectric anisotropy than the wurtzite structure of BN. Comparing our calculated data of $\epsilon(\infty)$ with those computed by the orthogonalized linear combination of atomic orbitals (OLCAO) (Refs. 29,56) and LMTO (Ref. 57) method we see that these procedures give systematically too small values. The OLCAO procedure, although very efficient for the calculation of the structural properties, seems not to be elaborated enough for accurate calculations of optical spectra. For 2*H* BN this procedure yields two quite different sets of the dielectric tensors,[29,56] whereas for 2*H* AlN the calculated large anisotropy $\Delta\epsilon(\infty)=0.276$ is too excessive.[56] The OLACO method predicts such disproportionately large anisotropies of $\epsilon(\infty)$ also for other wurtzite crystals SiC, GaN, InN, ZnO, and ZnS. In case of the LMTO method the underestimation of $\epsilon(\infty)$ may be traced back to the used atomic-sphere approximation, where the choice of the atomic-sphere radius influences the oscillator strengths, and the procedure used for the calculation of $\epsilon(\infty)$ via the Kramers-Kronig transformation from the optical spectrum. Moreover, both procedures neglect the influence of the local-field effects on the dielectric tensor which, as shown, lower the value of the dielectric constants by about 10–15 %. Our calculations of $\epsilon(\infty)$ for BN and AlN in both zinc-blende and wurtzite structures are, on the other hand, consistent with the LDA pseudopotential calculations of Chen *et al.* using a scissors operator for the energy of the conduction bands.[58]

The average values of the high-frequency dielectric tensors $\epsilon(\infty)$ of BN and AlN for both wurtzite and zinc-blende structures are rather similar; they differ by less than 2%. Therefore, both semiconductors exhibit similar electronic screening regardless of their different electronic band structures.[21,57,59] This somewhat surprising finding can be, however, explained by compensation effects between the average band gap $\overline{E_g}$ and the plasma frequency ω_p. According to the Penn formula for the dielectric constant the large averaged energy gap in BN, which is approximately related to the E_2 transition energy in the optical spectra, is counterbalanced by the high value of the plasma frequency. The ratio $\hbar\omega_p/\overline{E_g}$ has practically the same value for BN as for AlN.[60]

The (transverse) Born effective charge $Z^B(\kappa)$ represents the charge of the κth ion interacting with the macroscopic electric field. $Z^B(\kappa)$ is also referred to as *dynamic effective charge* as distinct from the *static effective charge* that results

from the static transfer of the electron charge density from the cation to the anion when a crystal is formed.[61] We note that the translational invariance of the crystal (the charge neutrality condition) imposes an important relationship between the components of the tensor of the Born effective charges that is known as the acoustic sum rule: $\Sigma_\kappa Z^{\mathrm{B}}_{\alpha\beta}(\kappa)=0$.[62] In the zinc-blende structure the tensor of the Born effective charges is isotropic: $Z^{\mathrm{B}}_{\alpha\beta}(\kappa)=Z^{\mathrm{B}}(\kappa)\,\delta_{\alpha\beta}$. The acoustic sum rule requires that there is only one independent component and the effective charge of the cation and ion are equal with opposite sign: $Z^{\mathrm{B}}=Z^{\mathrm{B}}(\mathrm{III})=-Z^{\mathrm{B}}(\mathrm{V})$. Although there are four atoms in the unit cell of the wurtzite structure the nonsymmorphic space group C^4_{6v} with a screw along the c axis enforces that only two of them are independent. Furthermore, because of the charge neutrality condition we have to consider only one tensor of Born effective charges with two independent components $Z^{\mathrm{B}}_{\perp}=Z^{\mathrm{B}}_{xx}(\mathrm{III})=Z^{\mathrm{B}}_{yy}(\mathrm{III})$ and $Z^{\mathrm{B}}_{\|}=Z^{\mathrm{B}}_{zz}(\mathrm{III})$.

Values of the calculated Born effective charges, in units of the electron charge, of $3C$ and $2H$ BN and AlN are listed in Table IV. The calculated values agree well with the experimental data obtained from first-order Raman-scattering experiments.[63] In our calculations the acoustic sum rule is fulfilled to better than 1% and represents, therefore, a stringent benchmark for the accuracy of the computations. To the best of our knowledge, no other first-principles calculations of the Born effective charges for BN and AlN exist. It has been already noticed by Luckovsky *et al.* that the values of the Born effective charges vary around $Z^{\mathrm{B}}=2$.[64] However, as can be seen in Fig. 3(a) chemical trends between the Born effective charges and the static ionicity coefficients for several III-V semiconductors are hardly visible. The situation changes dramatically when instead of the Born effective charge the screened effective charge $Z^*=Z^{\mathrm{B}}/\sqrt{\epsilon(\infty)}$ is considered. The values $Z^*=0.91$ for $3C$ BN and $Z^*=1.21$ for $3C$ AlN follow the trend given by the static ionicities, represented by the charge asymmetry coefficients $g=0.49$ for $3C$ BN and $g=0.80$ for $3C$ AlN. As shown in Fig. 3(b) a nearly linear relationship between Z^* and g can be established. Consequently, Z^* represents a better scale for the dynamic bond ionicity than Z^{B}.

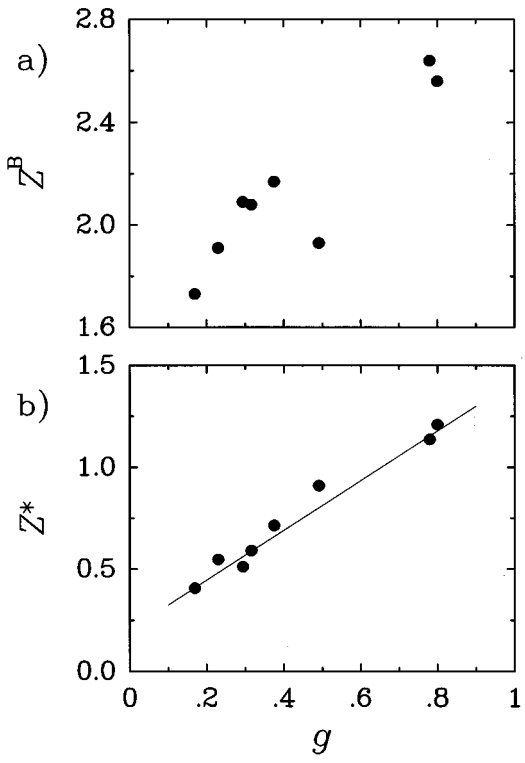

FIG. 3. (a) Calculated Born effective charges Z^{B} versus charge asymmetry coefficients g for several III-V zinc-blende compounds. The full circles plotted from the left to the right correspond to GaSb, AlSb, InSb, GaAs, AlAs, BN, GaN, and AlN. (b) Comparison of the screened charge Z^* with the static ionicity coefficient g. The solid line is a guide to the eye.

D. Vibrational properties

The results for the phonon dispersion curves of BN and AlN binary semiconductors in the zinc-blende structure are displayed in Fig. 4 along several high-symmetry lines together with the corresponding one-phonon density of states (DOS). For comparison the phonon frequencies and the one-phonon DOS of the isoelectronic counterparts of BN and AlN from the fourth column of the periodic table, diamond (C) and silicon carbide (SiC) are drawn. Very little is known about the vibrational properties of $3C$ BN for which only a few infrared and first-order Raman experiments exist.[63,65,66] The agreement between our computations and available experiments is excellent for C and SiC. It gives confidence in our results in the case of $3C$ BN, where a direct comparison with experiment is only possible for the zone-center (see Table V) and of $3C$ AlN, where no experimental data are available. The present parameter-free calculations stand, therefore, as reliable predictions for the full phonon dispersion curves of BN and AlN. The energy scales are mainly dominated by the different average masses of BN (C) and AlN (SiC). The dominant role of the first-row atoms for the lattice dynamics of AlN and BN is visible in the wave-vector dispersion of the phonon branches, which in the case of BN are very similar to those of diamond[12] and in the case of AlN to those of SiC.[47,67] In particular, the flatness of the TA branches over a large part of the BZ, which is typical for other III-V compounds as phosphides, arsenides, antimonides, partially (AlN) or widely (BN) disappears. Therefore, the pronounced peaks in the corresponding region of the one-phonon DOS are lacking. This fact indicates the occurrence of strong noncentral forces for the investigated compounds containing first-row elements. However, despite this similarity there are also several distinctions in the phonon dispersion curves of BN and AlN due to the different strengths of the elastic forces and the degree of the ionicity of both semiconductors.

Apart from the different magnitude of the LO-TO splitting at the zone-center due to the macroscopic electric field accompanying the polar longitudinal-optical-phonon modes, both semiconductors AlN and SiC exhibit roughly the same spectra. This is evident in the one-phonon DOS of both semiconductors, where the structures arising from the LO, TO, LA, and TA branches can be clearly separated. Because of the mass mismatch between aluminum and nitrogen (silicon and carbon), the optical branches, particularly the transverse one, are flat. As a result not only the acoustic and optical

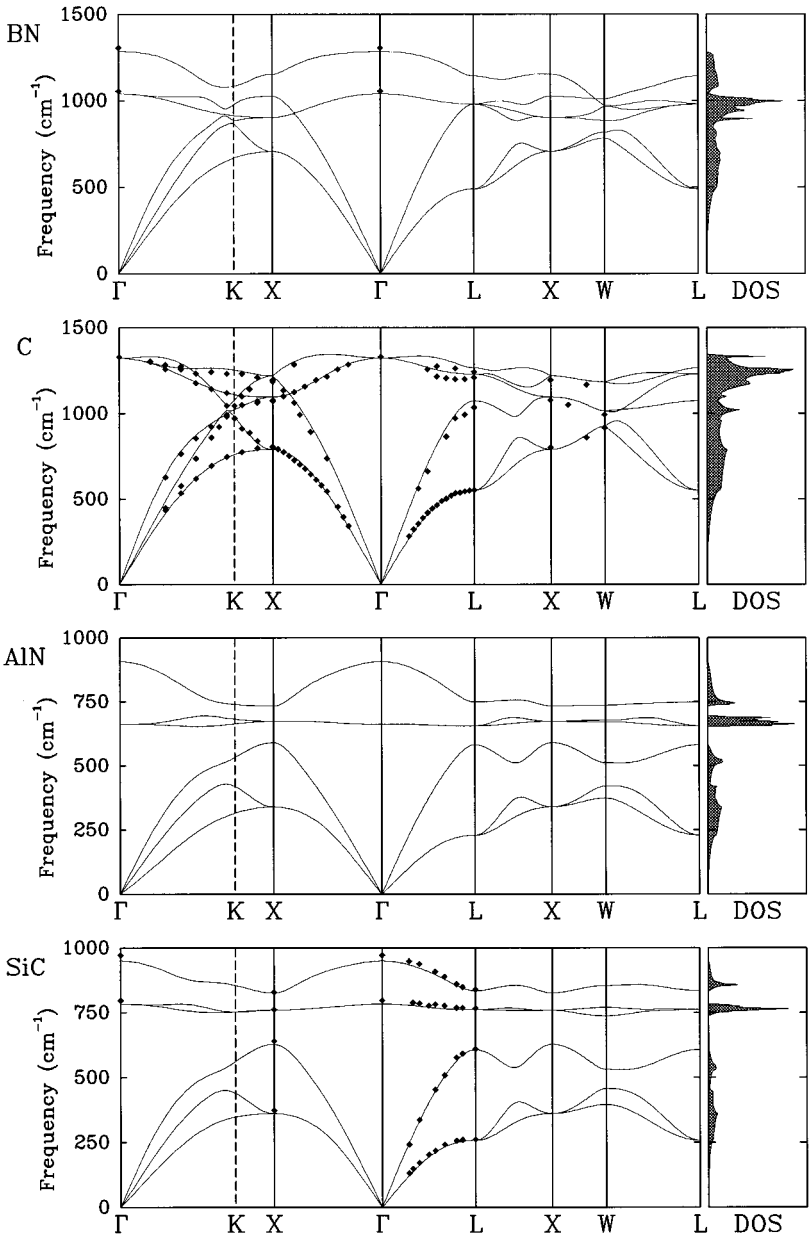

FIG. 4. Calculated phonon dispersion curves and the phonon density of states (DOS) for 3*C* BN and 3*C* AlN. For comparison the phonon frequencies and the DOS of the isoelectronic counterparts diamond and 3*C* SiC are shown. Experimental data from Ref. 63 are denoted by diamonds.

phonons are separated by a gap from 591 to 654 cm^{-1} for 3*C* AlN (from 628 to 737 cm^{-1} for 3*C* SiC) but also the transverse and the longitudinal optical phonon branches by a gap from 695 to 733 cm^{-1} for 3*C* AlN (from 784 to 827 cm^{-1} for 3*C* SiC).

The clear separation order of the acoustic- and optical-phonon branches does not occur in the one-phonon DOS of BN and diamond, since there is a considerable overlap between the LO-, TO-, and LA-phonon branches. This energetical overlap is caused by the (almost) identical masses of both atoms in the unit cell of diamond (BN). Although, there is a nonvanishing LO-TO splitting at the zone center, which is related to its partial ionic bonding, the phonon spectrum of BN, particularly considering the TO-, LA-, and TA-phonon branches, is quite similar to that of diamond. For the phonons propagating along the Σ ([110]) direction an interesting feature can be found in the phonon dispersion curves of both compounds: the anticrossing behavior of the acoustic and optical Σ_1 phonon branches. Because the Σ_1 phonon modes belong to the same representation, strong intermixing occurs near the *K* point. As a result the modes, which are not allowed to cross, show conspicuous features in the vicinity of the *K* point. On the other hand, one interesting peculiarity of the phonon spectrum of diamond, the occurrence of overbending of the LO-phonon mode[12]—i.e., regions in the Brillouin zone where the LO branch has higher frequency than at the zone center—is not observed in BN.

The phonon dispersion curves of BN and AlN in the wurtzite structure are plotted in Fig. 5 along the ΓA(Δ direction) and ΓKM (*T* direction) lines. The four atoms in the unit cell give rise to twelve phonon branches for a general **q** point. As can be seen in Fig. 5, this fact makes a detailed interpretation of the phonon dispersion curves for the wurtzite structure more complicated than for the zinc-blende structure. However, the group theoretical analysis of the phonon modes for a given **q** point is very helpful and can simplify the work exceedingly. The symmetry decomposition tells us, for instance, that along the Δ direction there are two Δ_1 and

TABLE V. Longitudinal and transverse zone-center phonon frequencies (in cm^{-1}) of BN and AlN in wurtzite and zinc-blende structures.

		2*H*				3*C*	
		E_1(LO)	A_1(LO)	E_1(TO)	A_1(TO)	LO	TO
	Present	1281	1258	1053	1006	1285	1040
	Calc. [a]						1004
	Calc. [b]						1063
	Calc. [c]						1071
BN	Expt. [d]						993
	Expt. [e]					1305	1055
	Expt. [f]					1304	1056
	Expt. [g]					1232	1000
	Expt. [h]					1305	1054
	Present	918	893	677	619	907	662
	Calc. [i]			649	629		652
	Calc. [j]			650	601		648
	Expt. [k]	913		670	610		
AlN	Expt. [l]	916	893	673	614		
	Expt. [m]	821	663	614			
	Expt. [n]	924			607		
	Expt. [h]	895	888	672	659		
	Expt. [f]	910	910	667	667		

[a]Pseudopotential, Wentzcovitch *et al.* (Ref. 26).
[b]Pseudopotential, Fahy (Ref. 78).
[c]Pseudopotential, Rodriguez-Hernandez *et al.* (Ref. 21).
[d]IR spectra, Chrenko (Ref. 74).
[e]First-order Raman spectra, Doll (Ref. 79).
[f]First-order Raman spectra, Brafman *et al.* (Ref. 66).
[g]First-order Raman spectra, Gelisse *et al.* (Ref. 65).
[h]First-order Raman spectra, Sanjurjo *et al.* (Ref. 63).
[i]LMTO, Gorczyca *et al.* (Ref. 80).
[j]Mix-basis approach, Miwa *et al.* (Ref. 77).
[k]First-order Raman spectra, Filippidis *et al.* (Ref. 70).
[l]First-order Raman spectra, McNeil *et al.* (Ref. 71).
[m]First-order Raman and IR spectra, Carlone *et al.* (Ref. 73).
[n]First-order Raman spectra, Perlin *et al.* (Ref. 72).

Δ_6 longitudinal branches and two double degenerate $\Delta_3^{(2)}$ and $\Delta_4^{(2)}$ transverse branches. At the A point the longitudinal and transverse modes are two times and four times degenerate ($2\times A_1^{(2)}$ and $2\times A_3^{(4)}$), respectively. Therefore, at the A point there are only four different frequencies to be calculated instead of 12 for a general **q** point. Along the T direction the group theory is less helpful, since there are only two different types of representations (T_1 and T_2) and both of them are one dimensional. Hence along this particular direction the twelve phonon branches exhibiting a spaghettilike behavior have to be calculated. At the Γ point the group theory predicts the decomposition of the phonon modes into the following representations: $1\times A_1+2\times B_1+1\times E_1+2\times E_2$. The A_1 and E_1 phonon modes are both Raman active and infrared active. The E_2 modes are only Raman active and the B_1 branches are silent. Therefore, according to the group theory, four Raman-active phonon modes are to be expected at the zone center. However, the group theory does not take into account the macroscopic electric field associated with the motion of the longitudinal-optical-phonon vibrations. The A_1 and E_1 modes are each split into LO and TO components, giving rise to a total of six Raman-active phonon modes.

In uniaxial crystals, the phonon frequencies of these extraordinary modes are angle dependent.[68,69] In Table V, the calculated frequencies of A_1 and E_1 modes are directly compared with the experimental data for both semiconductors under consideration. Keeping in mind the accuracy of our first-principles calculations of about 2%, the calculated frequencies of 2*H* AlN agree well with the recent first-order Raman-scattering data of Filippidis *et al.*,[70] McNeil *et al.*,[71] and Perlin *et al.*[72] The large scattering of the older data[63,66,73] should be mainly traced back to the strained epitaxial layers and their generally insufficient sample quality (see also Refs. 71 and 72). In the case of BN only infrared and first-order Raman frequencies for the cubic and the graphitelike phases have been measured.[63,66,74–76] The agreement of our DFPT results with other first-principles frozen-phonon computations for the nonpolar transverse modes is reasonable, particularly considering the variation of the frequencies due to the different lattice constants used.[57,77]

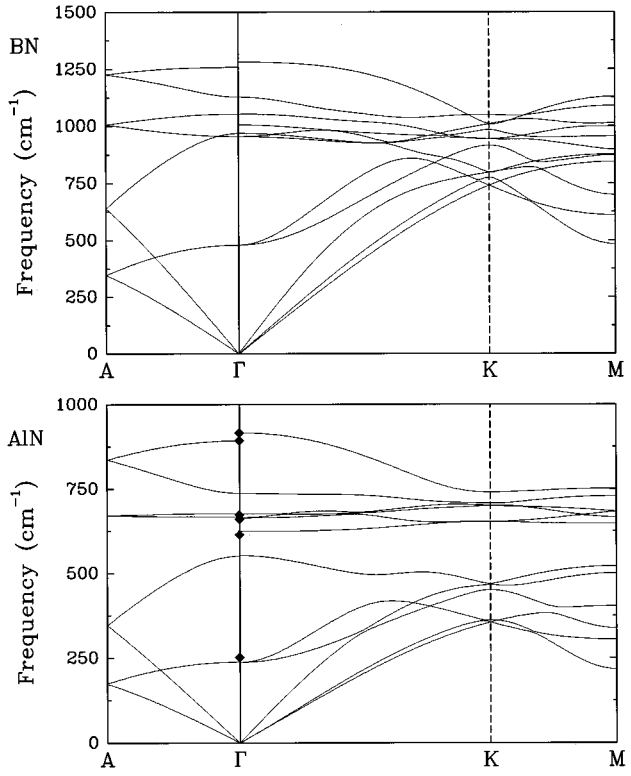

FIG. 5. Calculated phonon dispersion curves for 2*H* BN (upper panel) and 2*H* AlN (lower panel). Experimental first-order Raman-scattering data from Ref. 71 are denoted by diamonds.

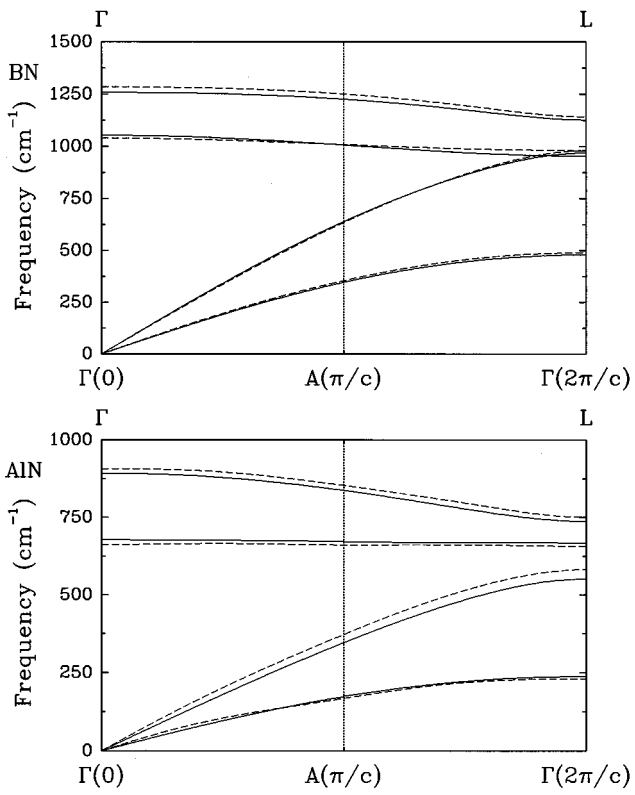

FIG. 6. Calculated phonon modes (solid lines) in the extended Jones zone for the Γ*A* direction of 2*H* BN (upper panel) and 2*H* AlN (lower panel). For comparison the phonon modes of 3*C* BN and 3*C* AlN along the Γ*L* direction are plotted as dashed lines.

According to Refs. 68 and 69, the uniaxial crystals can be divided into two different classes: class I, in which the electrostatic Coulomb forces dominate over the anisotropy of the short-range interatomic forces, and class II, in which the interatomic forces dominate over the electrostatic forces. In case of class I, the LO-TO splitting is more pronounced than the A_1-E_1 splitting. The opposite holds for class II, where the splitting between the A_1 and E_1 modes is much greater than the LO-TO frequency splitting. From Table V, we observe that $\omega(E_1(\mathrm{LO}))-\omega(E_1(\mathrm{TO}))=228\ \mathrm{cm}^{-1}$ for 2*H* BN (251 cm^{-1} for 2*H* AlN) and $\omega(A_1(\mathrm{LO}))-\omega(A_1(\mathrm{TO}))=252\ \mathrm{cm}^{-1}$ for 2*H* BN (274 cm^{-1} for 2*H* AlN). The splitting between the E_1 and A_1 modes amounts to $\omega(E_1(\mathrm{LO}))-\omega(A_1(\mathrm{LO}))=23\ \mathrm{cm}^{-1}$ for 2*H* BN (25 cm^{-1} for 2*H* AlN) and $\omega(E_1(\mathrm{TO}))-\omega(A_1(\mathrm{TO}))=47\ \mathrm{cm}^{-1}$ for 2*H* BN (58 cm^{-1} for 2*H* AlN). Therefore, both semiconductors BN and AlN belong to crystals of class II. It is interesting to note that the anisotropy of the tensor of the Born effective charges $\boldsymbol{Z}^{\mathrm{B}}(\kappa)$ and of the high-frequency dielectric tensor $\epsilon(\infty)$ lowers the frequency of the E_1(LO) mode from 1286 to 1281 cm^{-1} for 2*H* BN (from 924 to 918 cm^{-1} for 2*H* AlN) but raises the frequency of the A_1(LO) mode from 1248 to 1258 cm^{-1} for 2*H* BN (from 882 to 893 cm^{-1} for 2*H* AlN). The frequencies of other zone-center phonon modes are not affected by the anisotropy of $\boldsymbol{Z}^{\mathrm{B}}(\kappa)$ and $\epsilon(\infty)$. The ratio of $[E_1(\mathrm{TO})-A_1(\mathrm{TO})]/E_1(\mathrm{TO})$ may also be identified as a measure of crystal anisotropy for a given structure, i.e., wurtzite structure. This is indeed brought out by the calculated ratios of 4.5×10^{-2} for 2*H* BN and 8.6×10^{-2} for 2*H* AlN in comparison with the calculated (measured[81]) ratio 3.0×10^{-2} (3.6×10^{-2}) for 2*H* SiC, keeping in mind the more pronounced structural anisotropy (the distortion of the regular tetrahedra) of 2*H* BN and AlN (see Table I) than of 2*H* SiC.[13]

Considering the axial *c* direction, the wurtzite and zinc-blende structures differ only in the stacking order of double layers of atoms.[82] The sites of cations and anions in the unit cell of the wurtzite structure are not equivalent under primitive lattice translations, hence as discussed above there are twelve branches of the phonon spectrum in the BZ. However, the screw displacements and glide reflections along the axial direction of the nonsymmorphic space group C_{6v}^4 result in folding of the phonon modes along the Γ*A* line, the equivalent direction to the stacking direction of the double layers of atoms in direct space. Therefore, the phonon modes of the wurtzite structure along the Γ*A* direction can be directly compared with those of the zinc-blende structure along the equivalent Γ*L* direction using the scheme of the extended Jones zone.[83]

The calculated phonon-dispersion curves of the zinc-blende BN and AlN along the Γ*L* direction are plotted in Fig. 6 and compared with the unfolded phonon Γ*A* modes of the wurtzite structures (solid lines) of both semiconductors. The labels at the bottom of the plot correspond to the wurtzite and those at the top to the zinc-blende structure. The phonon branches of the wurtzite structure starting at the $\Gamma(0)$ point (zone center) go beyond the *A* point without discontinuity to the $\Gamma(2\pi/c)$ point at the edge of the large zone, which is the zone center of the next Brillouin zone. The wavelength of the phonon modes at the $\Gamma(2\pi/c)$ point

in the wurtzite structure is $\lambda = 2\pi/q = c$. The two inequivalent cations (anions) in the unit cell—each pair with a separation of $c/2$—vibrate out of phase. In contrast, in the $\Gamma(0)$ mode these inequivalent atoms vibrate in phase. The rather similar course of the phonon-dispersion curves of the zinc-blende and wurtzite structures of BN and AlN in the extended Jones zone is related to their structural similarities (see Table I). However, the frequencies of the phonon modes in both structures, particularly the longitudinal optic ones, are not as close as in the case of SiC.[47,84] Due to significant deviation of the ratio c/a of 1.657 for $2H$ BN and 1.605 for $2H$ AlN from its ideal value $\sqrt{8/3}$, the tetrahedra in the wurtzite structure of BN and AlN are more distorted than in $2H$ SiC. This structural distortion causes changes of the harmonic force constants of the different bonds of the wurtzite structure as compared to the zinc-blende structure. Therefore, the phonon frequencies of the unfolded phonon modes of the wurtzite structure, which describe the vibrations of the hexagonal double layers of atoms, depart from those of the equivalent modes of the zinc-blende structure. Another interesting feature, which may be related to the distortion of the tetrahedra in the wurtzite structure, is the closing of the energy gap between the TO- and LO-phonon modes of $2H$ AlN. As shown in Fig. 5 there is a slight overlap of these branches near the boundary of the hexagonal BZ, particularly in the neighborhood of the K point. The gap between the acoustic and optical modes exists at least for both calculated directions ΓA and ΓKM.

IV. CONCLUSIONS

In conclusion, we have presented *ab initio* calculations of ground-state, dielectric, and, in particular, of the lattice-dynamical properties of the group-III nitrides, AlN and BN, in both cubic (zinc-blende) and hexagonal (wurtzite) crystal modifications. The results for lattice constants, elastic coefficients, Born effective charges, dielectric constants, and Raman frequencies are in good agreement with the experimental data available. Despite the fact that both materials considered belong to group-III nitrides, their static and dielectric properties are rather different. These findings have been explained in terms of different relative and absolute strengths of the ionic versus the covalent bonding. Moreover, the lattice dynamics of BN and AlN differs considerably from that of other III-V semiconductors like GaAs, AlSb, or GaP. It has been found that the phonon spectrum of BN is close to that of diamond and the phonon spectrum of AlN close to that of SiC. This is a strong indication for the prominent role of the involved first-row element nitrogen for the bonding properties of both semiconductors. Furthermore, the different course of the phonon dispersion curves of BN and AlN cannot be explained by a simple mass approximation but is rather due to the quite different degree of the ionicity and strength of the covalent bonding of these semiconductors. Finally, the marked ionicity of the AlN bonding yields to a pronounced structural and dielectric anisotropy of the wurtzite structure of AlN larger than that of $2H$ BN and SiC.

ACKNOWLEDGMENTS

The authors wish to thank P. Pavone and D. Strauch for stimulating discussions. This work has been supported by the Deutsche Forschungsgemeinschaft under Contract No. Be 1346/8-1. A considerable part of the calculations have been performed on the Cray-YMP of the Forschungszentrum KFA in Jülich.

[1] R. S. Pearse, Acta Crystallogr. **5**, 536 (1952).
[2] V. L. Solozhenko, in *Properties of Group III Nitrides*, edited by J. H. Edgar (INSPEC, IEE, London, 1994).
[3] S. Porowski and I. Grzegory, in *Properties of Group III Nitrides* (Ref. 2).
[4] I. Petrov, E. Mojab, R. C. Powell, J. E. Greene, L. Hultman, and J.-E. Sundgren, Appl. Phys. Lett. **60**, 1491 (1992); M. J. Paisley and R. F. Davis, J. Cryst. Growth **127**, 136 (1993).
[5] P. Perdew and A. Zunger, Phys. Rev. B **23**, 5048 (1981).
[6] N. Troullier and J. L. Martins, Phys. Rev. B **43**, 1993 (1991).
[7] J. L. Martins, N. Troullier, and S.-H. Wei, Phys. Rev. B **43**, 2213 (1991); K. M. Glassford and J. R. Chelikowsky, *ibid.* **46**, 1285 (1992).
[8] D. J. Chadi and M. L. Cohen, Phys. Rev. B **8**, 5747 (1973).
[9] P. Vinet, J. Ferrante, J. R. Smith, and J. H. Rose, J. Phys. C **19**, L467 (1986).
[10] B. Baroni, P. Giannozzi, and A. Testa, Phys. Rev. Lett. **58**, 1861 (1987).
[11] P. Giannozzi, S. de Gironcoli, P. Pavone, and S. Baroni, Phys. Rev. B **43**, 7231 (1991).
[12] P. Pavone, K. Karch, O. Schütt, W. Windl, D. Strauch, P. Giannozzi, and S. Baroni, Phys. Rev. B **48**, 3156 (1993).
[13] K. Karch, F. Bechstedt, P. Pavone, and D. Strauch, Phys. Rev. B **54**, 13 400 (1996).
[14] T. Soma, S. Sawaoka, and S. Saito, Mater. Res. Bull. **9**, 755 (1974).
[15] E. Knittle, R. M. Wentzcovitsch, R. Jeanloz, and M. L. Cohen, Nature (London) **337**, 349 (1989).
[16] H. Schulz and K. H. Thiemann, Solid State Commun. **23**, 815 (1977).
[17] V. A. Pesin, Sverktverd. Mater. **6**, 5 (1980).
[18] I. Petrov, E. Mojab, R. C. Powell, J. E. Greene, L. Hultman, and J.-E. Sundgren, Appl. Phys. Lett. **60**, 2491 (1992).
[19] M. Ueno, A. Onodera, O. Shimomura, and K. Takemura, Phys. Rev. B **45**, 10 123 (1992).
[20] J. Furthmüller, J. Hafner, and G. Kresse, Phys. Rev. B **50**, 15 606 (1994).
[21] P. Rodriguez-Hernandez, M. Gonzales-Diaz, and A. Muonoz, Phys. Rev. B **51**, 14 705 (1995).
[22] K. Karch, T. Dietrich, W. Windl, P. Pavone, A. P. Mayer, and D. Strauch, Phys. Rev. B **53**, 7259 (1996).
[23] K. Karch, P. Pavone, A. P. Mayer, F. Bechstedt, and D. Strauch, Physica B **219&220**, 448 (1996).
[24] G. Cappellini, V. Fiorentini, K. Tenelsen, and F. Bechstedt, in *Gallium Nitride and Related Materials*, edited by R. D. Dupuis, J. A. Edmond, F. A. Ponce, and S. Nakamura, MRS Symposia Proceedings No. 395 (Materials Research Society, Pittsburgh, 1996).

[25] A. Satta, V. Fiorentini, A. Borin, F. Meloni, and D. Vanderbilt, in *Gallium Nitride and Related Materials* (Ref. 24).
[26] R. M. Wentzcovitsch, K. J. Chang, and M. L. Cohen, Phys. Rev. B **34**, 1071 (1986).
[27] R. M. Wentzcovitsch, M. L. Cohen, and P. K. Lam, Phys. Rev. B **36**, 6058 (1987).
[28] R. M. Wentzcovitsch, S. Fahy, M. L. Cohen, and S. G. Louie, Phys. Rev. B **38**, 6191 (1988).
[29] Y.-N. Xu and W. Y. Ching, Phys. Rev. B **44**, 7787 (1991).
[30] P. E. Van Camp, V. E. Van Doren, and J. T. Devreese, Phys. Rev. B **44**, 9056 (1991).
[31] P. E. Van Camp, V. E. Van Doren, and J. T. Devreese, Solid State Commun. **81**, 23 (1992).
[32] P. Lawaetz, Phys. Rev. B **5**, 4039 (1972).
[33] F. Bechstedt and P. Käckell, Phys. Rev. Lett. **75**, 2180 (1995).
[34] A. Garcia and M. L. Cohen, Phys. Rev. B **47**, 4215 (1993).
[35] G. Wellenhofer, K. Karch, P. Pavone, U. Rössler, and D. Strauch, Phys. Rev. B **53**, 6071 (1996).
[36] O. H. Nielson and R. M. Martin, Phys. Rev. Lett. **50**, 697 (1983).
[37] W. R. L. Lambrecht, B. Segall, M. Methfessel, and M. van Schilfgaarde, Phys. Rev. B **44**, 3685 (1991).
[38] L. Kleinman, Phys. Rev. **128**, 2614 (1962).
[39] K. Karch, Ph.D. thesis, Universität Regensburg, 1993.
[40] M. Grimsditch, E. S. Zouboulis, and A. Polian, J. Appl. Phys. **76**, 832 (1994).
[41] T. D. Sokolovskii, Inorg. Mater. **19**, 1311 (1983).
[42] R. C. De Vries, in *Cubic Boron Nitride: Handbook of Properties*, General Electric Report No. 72CRD178 (1972).
[43] K. Kim, W. R. L. Lambrecht, and B. Segall, Phys. Rev. B **53**, 16 310 (1996).
[44] E. Ruiz, S. Alvarez, and P. Alemany, Phys. Rev. B **49**, 7115 (1994).
[45] C. S. G. Cousins, L. Gerward, J. Staun Olsen, and B. J. Sheldon, J. Phys.: Condens. Matter **1**, 4511 (1989).
[46] C. N. Koumelis, G. E. Zardas, C. A. Londos, and D. K. Leventuri, Acta Crystallogr. A **32**, 84 (1975).
[47] K. Karch, P. Pavone, W. Windl, O. Schütt, and D. Strauch, Phys. Rev. B **50**, 17 054 (1994).
[48] R. M. Martin, Phys. Rev. B **6**, 4546 (1972).
[49] M. Hofmann, A. Zywietz, K. Karch, and F. Bechstedt, Phys. Rev. B **50**, 13 401 (1994).
[50] L. E. McNeil, M. Grimsditch, and R. H. French, J. Am. Ceram. Soc. **76**, 1132 (1993).
[51] K. Tsubouchi, K. Sugai, and N. Mikoshiba, in *1981 Ultrasonic Symposia Proceedings*, edited by B. R. McAvoy (IEEE, New York, 1981), p. 375.
[52] M. I. Eremets, M. Gauthier, A. Polian, J. C. Chervin, J. M. Besson, G. A. Dubitskii, and Ye. Ye. Semenova, Phys. Rev. B **52**, 8854 (1995).
[53] A. T. Collins, E. C. Leitowlers, and P. J. Dean, Phys. Rev. **158**, 833 (1967).
[54] L. Akasaki and M. Hashimoto, Solid State Commun. **5**, 851 (1967).
[55] A. Dal Corso, S. Baroni, and R. Resta, Phys. Rev. B **47**, 3588 (1993).
[56] Y.-N. Xu and W. Y. Ching, Phys. Rev. B **48**, 4335 (1993).
[57] N. E. Christensen and I. Gorczyca, Phys. Rev. B **50**, 4397 (1994).
[58] J. Chen, Z. Levine, and J. W. Wilkins, Appl. Phys. Lett. **66**, 1129 (1994).
[59] A. F. Wright and J. S. Nelson, Phys. Rev. B **51**, 7866 (1995).
[60] D. R. Penn, Phys. Rev. **128**, 2093 (1962).
[61] W. A. Harrison, *Electronic Structure and Properties of Solids* (Dover, New York, 1989).
[62] R. Pick, M. H. Cohen, and R. M. Martin, Phys. Rev. B **1**, 910 (1970).
[63] J. A. Sanjurjo, E. Lopez-Cruz, P. Vogl, and M. Cardona, Phys. Rev. B **28**, 5479 (1983).
[64] G. Luckovsky, R. M. Martin, and E. Burnstein, Phys. Rev. B **4**, 1367 (1971).
[65] P. J. Gelisse, S. S. Mitra, J. N. Plendl, R. D. Griffis, L. C. Mansur, R. Marshall, and E. A. Pascoe, Phys. Rev. **155**, 1039 (1967).
[66] O. Brafman, G. Lengyel, S. S. Mitra, P. J. Gielisse, J. N. Plendl, and L. C. Mansur, Solid State Commun. **6**, 523 (1968).
[67] K. Karch, P. Pavone, W. Windl, D. Strauch, and F. Bechstedt, Int. J. Quantum Chem. **56**, 801 (1995).
[68] R. Loudon, Adv. Phys. **13**, 423 (1964).
[69] D. W. Feldman, J. H. Parker, Jr., W. J. Choyke, and L. Patrick, Phys. Rev. **173**, 787 (1968).
[70] L. Filippidis, H. Siegle, A. Hoffmann, C. Thomsen, K. Karch, and F. Bechstedt, Phys. Status Solidi B **198**, 621 (1996).
[71] L. E. McNeil, M. Grimsditch, and R. H. French, J. Am. Ceram. Soc. **76**, 1132 (1993).
[72] P. Perlin, A. Polian, and T. Suski, Phys. Rev. B **47**, 2874 (1993).
[73] C. Carlone, K. M. Lakin, and H. R. Shanks, J. Appl. Phys. **55**, 4010 (1984).
[74] R. M. Chrenko, Solid State Commun. **14**, 511 (1974).
[75] R. Geick, C. H. Perry, and G. Rupprecht, Phys. Rev. **146**, 543 (1974).
[76] G. J. Exarhos and J. W. Schaaf, J. Appl. Phys. **69**, 2543 (1991).
[77] K. Miwa and A. Fukumoto, Phys. Rev. B **48**, 7897 (1993).
[78] S. Fahy, Phys. Rev. B **51**, 12 873 (1995).
[79] G. L. Doll, in *Properties of Group III Nitrides* (Ref. 2).
[80] I. Gorczyca, N. E. Christensen, E. L. Pletzer y Blanca, and C. O. Rodriguez, Phys. Rev. B **51**, 11 936 (1995).
[81] S. Nakashima, A. Wade, and Z. Inoue, J. Phys. Soc. Jpn. **56**, 3375 (1987).
[82] A. R. Verma, *Crystal Growth and Dislocations* (Butterworths Scientific Publications Ltd., London, 1953).
[83] H. Jones, *The Theory of Brillouin Zone and Electronic States* (North-Holland, Amsterdam, 1960).
[84] S. Nakashima and K. Tahara, Phys. Rev. B **40**, 6339 (1989).